AGU PUBLICATIONS

JGR

Journal of Geophysical Research: Space Physics

RESEARCH ARTICLE
10.1002/2015JA022307

Key Points:
- ICME complexity increases due to interaction with corotating structures in the solar wind
- Magnetic reconnection between ICME and HPS/HCS alters the magnetic topology of the ICME flux rope
- Caution on using distant observations to predict the geoeffectiveness of interplanetary transients

Correspondence to:
R. M. Winslow,
reka.winslow@unh.edu

Citation:
Winslow, R. M., N. Lugaz, N. A. Schwadron, C. J. Farrugia, W. Yu, J. M. Raines, M. Leila Mays, A. B. Galvin, and T. H. Zurbuchen (2016), Longitudinal conjunction between MESSENGER and STEREO A: Development of ICME complexity through stream interactions, *J. Geophys. Res. Space Physics*, *121*, 6092–6106, doi:10.1002/2015JA022307.

Received 23 DEC 2015
Accepted 19 JUN 2016
Accepted article online 24 JUN 2016
Published online 19 JUL 2016

Longitudinal conjunction between MESSENGER and STEREO A: Development of ICME complexity through stream interactions

Reka M. Winslow[1], Noé Lugaz[1], Nathan A. Schwadron[1], Charles J. Farrugia[1], Wenyuan Yu[1], Jim M. Raines[2], M. Leila Mays[3,4], Antoinette B. Galvin[1], and Thomas H. Zurbuchen[2]

[1]Institute for the Study of Earth, Ocean, and Space, University of New Hampshire, Durham, New Hampshire, USA, [2]Department of Climate and Space Sciences and Engineering, University of Michigan, Ann Arbor, Michigan, USA, [3]Catholic University of America, Washington, District of Columbia, USA, [4]Heliophysics Science Division, NASA Goddard Space Flight Center, Greenbelt, Maryland, USA

Abstract We use data on an interplanetary coronal mass ejection (ICME) seen by MErcury Surface, Space ENvironment, GEochemistry, and Ranging (MESSENGER) and STEREO A starting on 29 December 2011 in a near-perfect longitudinal conjunction (within 3°) to illustrate changes in its structure via interaction with the solar wind in less than 0.6 AU. From force-free field modeling we infer that the orientation of the underlying flux rope has undergone a rotation of ~80° in latitude and ~65° in longitude. Based on both spacecraft measurements as well as ENLIL model simulations of the steady state solar wind, we find that interaction involving magnetic reconnection with corotating structures in the solar wind dramatically alters the ICME magnetic field. In particular, we observed a highly turbulent region with distinct properties within the flux rope at STEREO A, not observed at MESSENGER, which we attribute to interaction between the ICME and a heliospheric plasma sheet/current sheet during propagation. Our case study is a concrete example of a sequence of events that can increase the complexity of ICMEs with heliocentric distance even in the inner heliosphere. The results highlight the need for large-scale statistical studies of ICME events observed in conjunction at different heliocentric distances to determine how frequently significant changes in flux rope orientation occur during propagation. These results also have significant implications for space weather forecasting and should serve as a caution on using very distant observations to predict the geoeffectiveness of large interplanetary transients.

1. Introduction

Coronal mass ejections (CMEs) are large eruptions of plasma and magnetic field into interplanetary space originating in the Sun's atmosphere [e.g., *Cane and Richardson*, 2003; *Zurbuchen and Richardson*, 2006]. The interplanetary counterparts of CMEs are known as interplanetary coronal mass ejections (ICMEs), and fast ICMEs are most often characterized by a leading shock wave followed by a dense sheath and a magnetic flux rope at the center of the disturbance. ICMEs are common, passing over Earth at an approximate rate of 1–2 per month [*Lynch et al.*, 2003; *Richardson and Cane*, 2010], although this number is significantly higher near the maximum phase of the solar cycle.

At Earth, the effects of ICMEs on the magnetosphere have been studied for many decades (e.g., review by *Singh et al.*, 2010). Because ICMEs can be associated with strong southward interplanetary magnetic fields of long duration, high solar wind velocities, enhanced solar wind dynamic pressures, and solar energetic particles, they are strong drivers of geomagnetic storm activity at Earth [e.g., *Lindsay et al.*, 1995; *Farrugia et al.*, 1997]. Geomagnetic storms are caused by the transfer of momentum and energy from the solar wind to the magnetosphere during times of southward directed interplanetary magnetic fields, when magnetic reconnection can occur between the oppositely directed fields of the interplanetary magnetic field (IMF) and Earth [e.g., *Russell et al.*, 1974; *Farrugia et al.*, 1993]. Using space-based observations, *Gonzalez and Tsurutani* [1987] have shown that ICMEs with southward pointed magnetic fields greater than 10 nT and lasting longer than approximately 3 h lead to intense ($Dst < -100$ nT) magnetic storms, where the *Dst* index is a measure of the strength of the ring current around the Earth.

The geoeffectiveness, or the storm-causing ability, of ICMEs strongly depends on the magnetic field direction within them. ICMEs are strong drivers of geomagnetic activity, as a statistical study by *Zhang et al.* [2004]

showed that 70% of intense storms are caused by ICMEs. However, only about 20% of Earth-directed solar ejecta cause intense geomagnetic storms [*Tsurutani et al.*, 1988]. The rest either do not have substantial southward directed fields or have highly time-varying magnetic fields, i.e., do not have strong southward directed fields for more than 3 h. Thus, successfully predicting the occurrence and intensity of geomagnetic storms based on magnetic field measurements relies on the ability to measure the orientation of the magnetic field in the ICME and its duration prior to it reaching Earth, provided that the magnetic field direction does not change drastically during the remaining propagation time. A recent proof-of-concept study by *Kubicka et al.* [2015] based on one ICME event shows that such predictions are possible, although further work is needed to establish the conditions under which they are valid.

ICME properties can change drastically as the ICME propagates through the solar wind. The speed, density, pressure, magnetic field, and shock structure can all change as the ICME expands and interacts both with the ambient solar wind as well as with various disturbances within it. In particular, through observational and modeling work, studies have shown that during propagation the flux rope may kink and deform [*Manchester et al.*, 2004], reconnection/erosion of internal ICME magnetic flux may occur [*Lavraud et al.*, 2014; *Ruffenach et al.*, 2015], and the ICME may also get deflected [*Manchester et al.*, 2005; *Kay et al.*, 2013, 2015; *Wang et al.*, 2014] and rotated [*Kliem et al.*, 2012; *Lynch et al.*, 2009]. A recent CME event study by *Nieves-Chinchilla et al.* [2012] using both in situ and remote sensing observations from STEREO, SOHO, MErcury Surface, Space ENvironment, GEochemistry, and Ranging (MESSENGER), and Wind showed evidence for significant reorientation of the flux rope axis. Similarly, *Rouillard et al.* [2009] showed that the trailing part of a particular ICME displayed highly distinct magnetic signatures at MESSENGER compared to measurements at Venus Express, despite the very small (~1°) longitudinal separation between the two spacecraft. On the other hand, an in situ study by *Good et al.* [2015] of an ICME observed in near-perfect conjunction at Mercury and STEREO B has showcased an event where the large-scale magnetic field structure evolution in the magnetic cloud (MC) remains self-similar during propagation. In situ multipoint measurements by *Möstl et al.* [2012] of a series of ICME events also show similarities between the flux ropes observed by Venus Express and STEREO B, despite the ~18° longitudinal separation between the spacecraft.

The varied results of these studies raise the question: what causes some ICME flux ropes to change drastically during propagation while others stay relatively self-similar? These past works therefore highlight the need for further exploration of evolution of the ICME magnetic field structure during propagation. Now, with 5 years of MESSENGER measurements near Mercury's orbit as well as continuous spacecraft measurements at 1 AU, such studies are possible for the first time in the innermost heliosphere. Also, a new era of inner heliosphere exploration from in situ measurements is expected to begin with the launch of Solar Orbiter [*Müller and St. Cyr*, 2013] and Solar Probe Plus [*Fox et al.*, 2015] in the next 3 years. Due to their proximity to the Sun, these spacecraft (will) present a unique opportunity for observing ICMEs in more "pristine" conditions, well before they reach 1 AU.

In this paper, we present a study of a CME launched from the Sun on 29 December 2011, and we follow its propagation from the Sun to 1 AU. Due to the MESSENGER/STEREO A directed nature of the ICME, and the near-perfect alignment between these spacecraft at this time, one would expect close agreement of flux rope parameters at the two locations. Instead, due to the interaction of the ICME with the heliospheric plasma sheet (HPS) and current sheet (HCS) between Mercury and STEREO A, a very different ICME magnetic field structure is observed at the two spacecraft. The observations and analyses present a concrete example of a scenario where ICME interaction with corotating structures in the solar wind significantly alters the flux rope magnetic topology and increases the complexity of the ICME during propagation. Based on these results, our paper is a caution on using magnetic field measurements close to the Sun for geomagnetic storm forecasting at Earth when corotating structures are present in the Sun-to-Earth transit space. Large-scale statistical studies of ICME magnetic field changes from the innermost heliosphere to 1 AU are also necessary to determine the frequency with which drastic alterations in flux rope orientation occur due to solar wind interactions.

2. The 29 December 2011 CME

The CME was launched from the Sun at or around 15:52 UT on 29 December 2011 and was observed by coronagraphs on board both STEREOs and SOHO. STEREO A Extreme Ultraviolet Images (EUVI) observations show a filament eruption from disk center with the rising phase starting around 15:00 UT. At this time, STEREO A was ~107° west of the Sun-Earth line, while STEREO B was ~111° east of the Sun-Earth line. The first observation

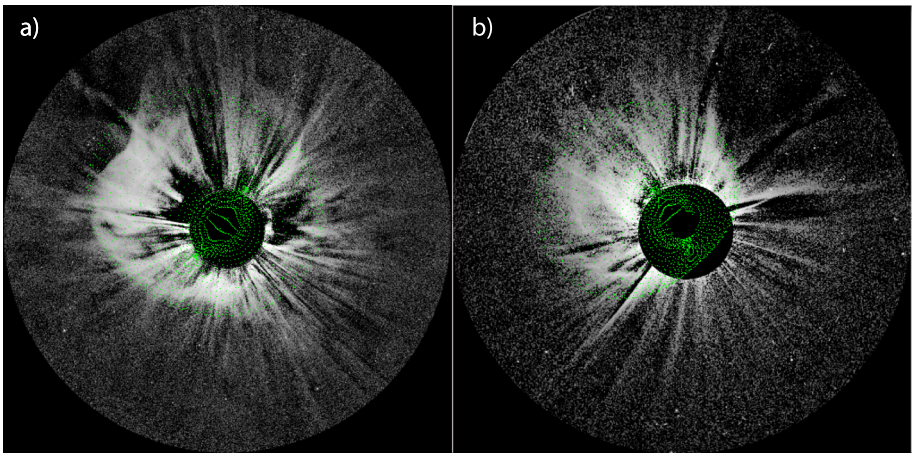

Figure 1. COR2 (a) STEREO A and (b) STEREO B white light images (at 19:08:15 on 29 Dec. 2011) with an overlay in green of the GCS wireframe. Figure credit: http://www.affects-fp7.eu/ helcats-database.

by the Outer Coronagraph (COR2) on the Sun Earth Connection Coronal and Heliospheric Imaging (SECCHI) package on STEREO of the CME was at 17:24 UT and appeared as a front halo CME, i.e., it was directed at STEREO A. The same event was also observed as a back-sided halo by STEREO B/COR2. The Large Angle and Spectrometric Coronagraph (LASCO) on SOHO observed a wide western limb CME (first image 16:24 UT). Since it is a limb CME for LASCO, this instrument provides the best estimate of the CME onset and speed, 15:52 UT and 750 km s^{-1}, respectively. The COR2 maximum speeds were 540 and 780 km s^{-1} for STEREO A and B, respectively.

Due to the near-perfect alignment (within 3° longitude) of MESSENGER and STEREO A between the time of the CME launch on 29 December 2011 and its arrival at STEREO A on 1 January 2012, the CME was observed in situ at both spacecraft. At this time, Mercury's heliocentric distance was 0.42 AU, while the STEREO A heliocentric distance was 0.96 AU. With a speed of 750 km s^{-1}, and assuming no deceleration, this CME would arrive at Mercury 23 h after its launch, or at ~14:50 UT on 30 December, and at ~21:00 UT on 31 December at STEREO A. Taking into account uncertainties in the estimated speed and the expected deceleration of the CME in the solar wind, this CME has the required timing characteristics to correspond to the ICME and shock measured at MESSENGER on 30 December starting at 16:27 UT (~1.5 h "late") and to correspond to the ICME measured at STEREO A arriving at 13:22 UT (~16.5 h "late") on 1 January. We note that these arrival timing differences are quite minor given the assumption of constant velocity. Additionally, we perform a more complete analysis of the CME kinematics at the end of section 3.

The graduated cylindrical shell (GCS) model [*Thernisien et al.*, 2006, 2011] was designed to reproduce the large-scale structure of flux rope-like CMEs and determines the initial orientation of the flux rope soon after launch. To this end, we use the GCS fit from the STEREO/SECCHI/COR2 CME Kinematic Database (KINCAT) of the Institute for Astrophysics, University of Göttingen, Germany. The database is available online at http://www.affects-fp7.eu/helcats-database. The GCS fit of this CME as seen from STEREO A (Figure 1a) and B (Figure 1b) SECCHI data (using white light images from 29 December at 19:08 UT) finds that the flux rope longitude was 98° ± 4°, the latitude was 7° ± 2°, with a tilt angle of −36° ± 22°. At this time, STEREO A was at a longitude of 107°, so this implies that the CME initial flux rope orientation was only 9° away from the Sun-MESSENGER-STEREO A line, toward the east, i.e., toward the Sun-Earth line. These results forecast the CME to be hitting MESSENGER and STEREO A nearly head-on.

(i) The longitudinal alignment between MESSENGER and STEREO A, (ii) the initial direction of the CME determined to be within ~ 10° of STEREO A, (iii) the arrival time of the ICME matching quite closely with the expected arrival times at the two spacecraft, and (iv) the same chirality of the flux rope observed at the two spacecraft (see section 3 below) all support the hypothesis that the measurements at MESSENGER and STEREO A are of the same ICME. Using the method of coplanarity [e.g., *Schwartz*, 1998], we have determined the shock normal direction in heliospheric radial-tangential-normal (RTN) coordinates at both spacecraft and found $\hat{n}$ = (0.77, 0.20, 0.61) at MESSENGER and $\hat{n}$ = (0.71, 0.18, 0.68) at STEREO A, yielding a 5° difference between the two shock

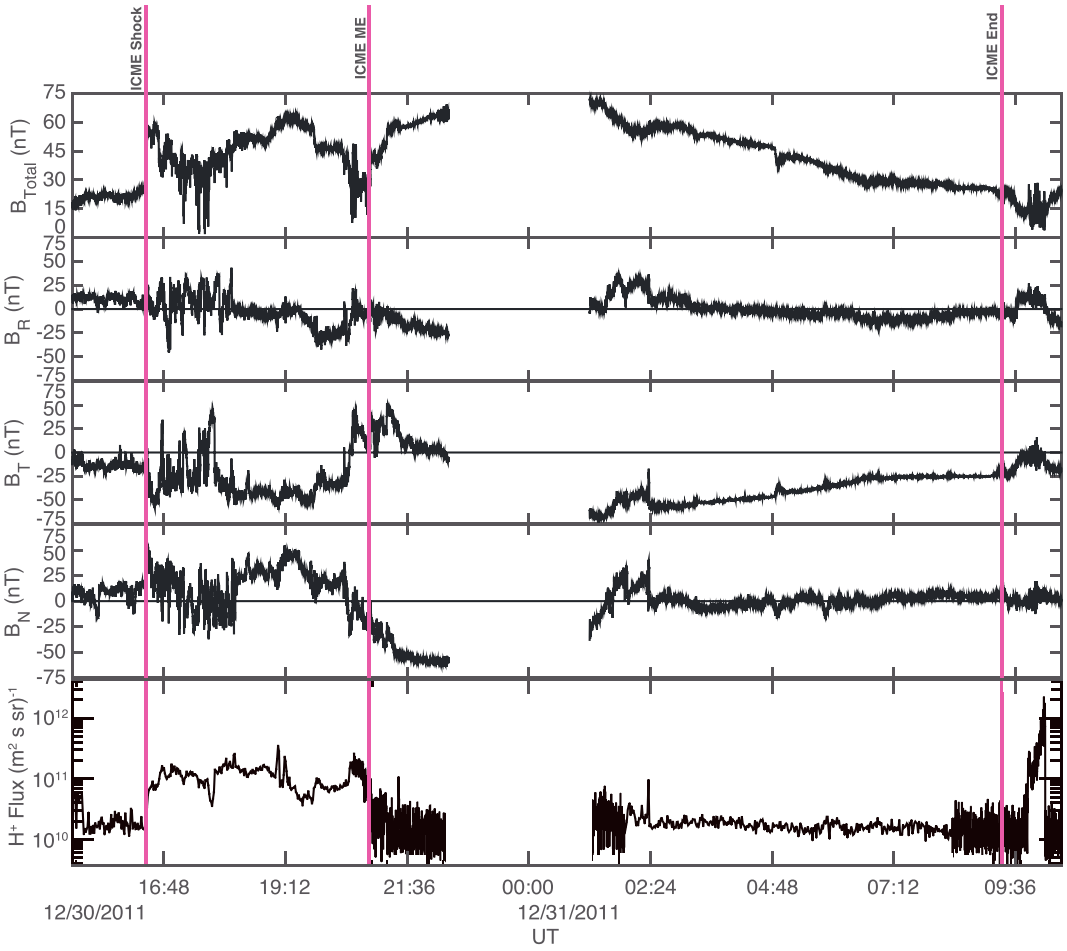

Figure 2. MESSENGER measurements of the ICME on 30-31 December 2011. The first four panels show magnetic field data in RTN coordinates. The last panel shows FIPS data of the proton flux over the same time period. Vertical magenta lines denote the crossing time of the ICME shock, magnetic ejecta, and ICME end. The data gap corresponds to MESSENGER's passage through Mercury's magnetosphere. For this event, the ICME end was marked by a small discontinuity or reverse shock (not visible at this scale on the figure).

normal directions. The very close agreement between the shock normals provides further evidence that the measurements at the two spacecraft are of the same ICME.

2.1. MESSENGER Data

At Mercury, the ICME was observed in MESSENGER magnetic field data. Due to its highly eccentric orbit, during this time MESSENGER typically spent 8–10 h of its 12 h orbit in the interplanetary medium. Magnetometer sample rates in the interplanetary medium were at least as high as 2 samples/s and a channel to record fluctuations at 1–10 Hz operated continuously to provide an uninterrupted measure of the field variability. Although the MESSENGER payload included a plasma spectrometer (the Fast Imaging Plasma Spectrometer (FIPS)) [see *Andrews et al.*, 2007], the spacecraft was three axis stabilized and FIPS had a limited field of view that did not allow for the recovery of the solar wind density. Solar wind speed and temperature could be derived from the measurements about 50% of the time that MESSENGER was in the solar wind [*Gershman et al.*, 2012].

In *Winslow et al.* [2015] we describe in detail the strict selection criteria used to identify ICME events from only magnetic field measurements. Due to the strong magnetic field and shock associated with this ICME and the smooth magnetic field rotation in the magnetic ejecta (ME), an ICME is easily discernible in the data. Figure 2 shows the ICME event in the MESSENGER magnetic field data, displayed in RTN coordinates. The ICME shock arrived on 30 December at 16:27:23 UT (first magenta vertical line in Figure 2), followed by the sheath region and ME. The ME start time of 20:52:38 UT is ~3 h later than our initial choice shown in *Winslow et al.* [2015], yielding a total sheath crossing time of ~5 h (bracketed by the first two vertical magenta guidelines). After

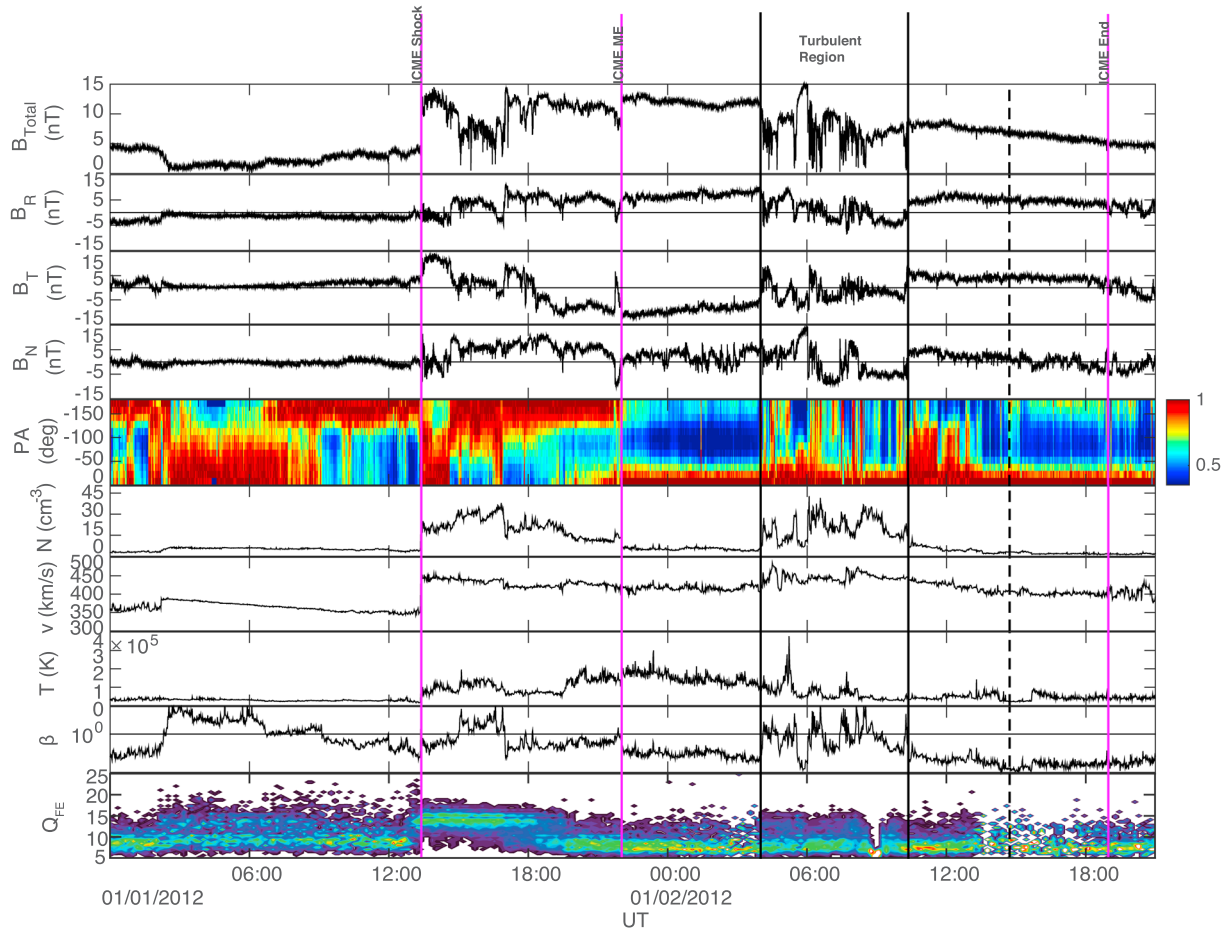

Figure 3. STEREO A magnetic field and plasma data of the ICME on 1–2 January 2012. (top to bottom) The magnetic field magnitude, the magnetic field vector components in RTN coordinates, suprathermal electron pitch angle distributions, the proton density, velocity, temperature, the plasma β, and the 10 min averaged iron charge state distribution over the time period. Vertical magenta lines denote the crossing time of the ICME shock, magnetic ejecta, and ICME end, while the black vertical lines denote the start and end of the turbulent region. The black dashed line indicates the time of the return to bidirectional electron flows in the magnetic ejecta.

careful consideration, in light of partial FIPS data of the solar wind, we revised the start of the ME such that the sheath still includes the highly turbulent region between ~19:45 and ~20:50 UT. A simple analysis of the magnetic field latitude versus longitude shows that this turbulent region exhibits a very clear planar structure (i.e., the magnetic field varies strictly in a plane), which is expected for ICME sheaths [*Palmerio et al.*, 2016]. Furthermore, Figure 2 (fifth panel) shows a fairly steady cumulative proton count from the time of the ICME arrival until ~20:45 UT, at which time there was a distinct and sustained drop in the flux coinciding quite closely in time with the beginning of the smooth magnetic field rotation, signaling a transition from ICME sheath to ME. MESSENGER then crossed Mercury's magnetosphere between 22:25:12 UT and 01:12:02 UT on 31 December. Once MESSENGER reemerged into the interplanetary medium, the proton flux was still low, in agreement with the magnetic field measurements that MESSENGER was once again in the ME portion of the ICME. The magnetic field in this ICME flux rope is characterized by low magnetic fluctuations, and a rotation of the magnetic field vector is observed in the B_T and B_N components, with B_T being the dominant field component in the ME. The end of the ME at 09:19:52 UT (last vertical magenta line in Figure 2) was marked by a discontinuity, possibly a weak reverse shock.

2.2. STEREO A Data

In this section, our aim is to focus on STEREO A data of the ICME only, while in section 4, we discuss at length the STEREO A measurements prior to the ICME, as well as the background solar wind both from data and simulations. At 1 AU, STEREO A data show the ICME to be significantly more disturbed than at MESSENGER. The In situ Measurements of Particles And CME Transients (IMPACT) [*Luhmann et al.*, 2008] and Plasma And

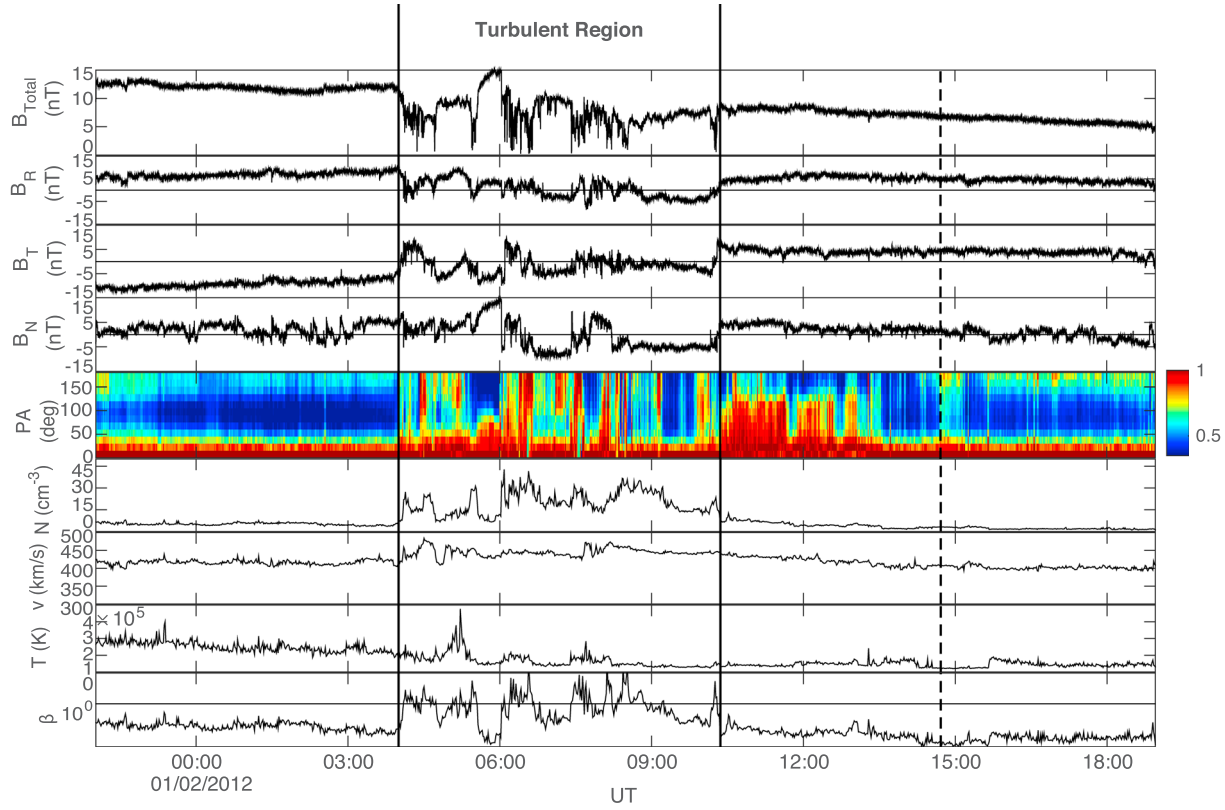

Figure 4. STEREO A magnetic field and plasma data of the magnetic ejecta. (top to bottom) The magnetic field magnitude, the magnetic field vector components in RTN coordinates, suprathermal electron pitch angle distributions, the proton density, velocity, temperature, and the plasma β. The vertical black lines denote the start and end of the turbulent region, while the black dashed line indicates the time of the return to bidirectional electron flows in the ME.

Suprathermal Ion Composition (PLASTIC) [*Galvin et al.*, 2008] packages on the STEREO spacecraft were specifically designed to provide in situ measurements of ICMEs including magnetic field observations and 3-D distributions of the solar wind plasma. Figure 3 shows STEREO A data (magnetic field, suprathermal electron pitch angle distributions, density, velocity, temperature, plasma β, and the iron charge state distribution) of the ICME. Suprathermal electron pitch angle distributions have been normalized at each time step and represent cumulative electron fluxes over all energies between 45 and 2188 eV. Iron charge state data are accumulated in 10 min intervals, plotted at the beginning of the interval. The ICME shock arrival at 13:23:44 UT on 1 January 2012 is marked by a clear jump in the magnetic field magnitude, coincident with jumps in plasma density, velocity, and temperature. Then STEREO A spent ~8.6 h in the ICME sheath (between the first two magenta vertical guidelines in Figure 3) where the magnetic field strength and direction were highly variable. The suprathermal electron pitch angle distributions exhibit an abrupt change from the 180° strahl component to unidirectional flows in the opposite direction at the shock, followed by mostly unidirectional but also some bidirectional flows in the sheath. A clear sustained drop in plasma density, the onset of sustained bidirectional suprathermal electrons, and the start of smooth magnetic field rotations indicate the arrival of the ME portion of the ICME at 22:00:57 UT on 1 January 2012.

The ME portion of the ICME (between the second and third magenta lines and shown in higher resolution in Figure 4), which lasted from 22:00:57 UT on 1 January 2012 until 18:57:45 on 2 January 2012, exhibits a smooth rotation in the magnetic field direction and low variability magnetic field in general, with B_R and B_T being the dominant magnetic field components. However, near the center of the ME crossing, a region with different properties compared with the rest of the ME was encountered on 2 January at 04:00:00 and lasted until 10:21:26 UT (marked by black vertical lines in Figure 3). This turbulent region is characterized by high magnetic field fluctuations, high plasma density, an increase in velocity, fluctuating temperature, and a small increase in the average iron charge state. The increase in average iron charge state implies a different source for the plasma in this region than for the rest of the ME, while the overall increased value of plasma β in the region strongly implies plasma heating. We have also tested that this turbulent region is not a planar structure.

Plasma velocity measurements show a change in polarity in the tangential component of the velocity vector, v_T (not shown here), just at the start of the turbulent region. A change in sign of the azimuthal flow angle, for which v_T is a proxy, indicates a stream interface [*Gosling and Pizzo*, 1999]. The measurements also indicate that there is likely a slow mode shock near 06:00 UT due to the sharp increase in density, temperature, and velocity, along with a corresponding sharp decrease in magnetic field magnitude. The combination of these data in this distinct region hints at signatures of reconnection, which likely occurred between the flux rope and the HPS/HCS that the ICME overtook during propagation (see section 4).

The strongest case for signatures of reconnection in this region, however, is made by the suprathermal electrons. Within the ME, both before and after the turbulent region, STEREO A measured counter-streaming electrons, while within the region, the pitch angle distribution was highly variable. There are clear intervals when bidirectional flows are detected but they are interspersed with sharp drop-outs to unidirectional flows only. This alternating signature of short bursts of bidirectional then unidirectional flows implies the succession of closed to open field lines (i.e., both ends connected at the Sun or only one end connected), indicating interchange reconnection. We discuss the implications of these signatures further in sections 4 and 5 of the paper.

It is also worth mentioning, that even though a return to the smooth rotation in the magnetic field direction, low plasma density, and decrease in plasma velocity and plasma β indicate the return to the nonturbulent part of the ME at ~10:20 UT, sustained counter-streaming suprathermal electrons only return ~4 h later, marked by the dashed vertical line in Figures 3 and 4. STEREO A then spent another ~8.5 h in the ME, which displayed similar properties to those observed prior to the encounter of the turbulent region. The end of the ME passage (last magenta vertical guideline) was identified based on the start of large magnetic field fluctuations and the end of the steady magnetic field magnitude decrease. However, since there are no clear indicators in the plasma data, the ICME end time carries some uncertainty.

Due to the interruption of the ME by the turbulent region, the question whether there are actually two distinct flux ropes from two separate ICMEs, naturally arises. This hypothesis, although plausible at first sight, fails to explain several measurements. First, MESSENGER only observes one flux rope at Mercury. Second, if separated, the duration of each flux rope (excluding the turbulent region) at STEREO A (~6 h and ~8 h) is much shorter than the flux rope duration observed at Mercury (~12 h), which is contrary to the expectation that ICMEs expand as they propagate outward in the solar system. Lastly, if separated, neither flux rope would actually meet the definition of a flux rope given that neither on its own exhibits a smooth rotation in **B**. Thus, our initial scenario, that there is only one flux rope, which underwent reconnection with corotating disturbances in the solar wind, is the most likely scenario.

3. Force-Free Field Fitting and ICME Speed

Initial comparison between the large-scale magnetic field structure in the ME at MESSENGER and at STEREO A shows that rotation in the magnetic field occurred during propagation. To quantify the change in the magnetic field direction, we determined the flux rope orientation at the two spacecraft by conducting force-free field fits to the data. Here the model used is a nonexpanding, constant α force-free field model as developed by *Burlaga* [1988], and we used a χ^2 minimization procedure as optimized by *Lepping et al.* [1990]. The flux rope axis orientation is first evaluated via minimum variance analysis, which is then used as the starting point for the force-free field fits. For the fits at 1 AU, we did not include data during the highly turbulent interval in the ME between 04:06:45 and 10:20:50 UT.

The force-free field fits (Figure 5) yield a left-handed flux rope at both spacecraft, with $\theta = -12.3° \pm 0.4°$, $\phi = 131° \pm 1°$, and $B_0 = 55.9 \pm 0.5$ nT at MESSENGER, and $\theta = 66° \pm 5°$, $\phi = 197° \pm 8°$, and $B_0 = 12.3 \pm 0.5$ nT at STEREO A, where the uncertainties represent 3 sigma statistical errors. Here θ is the angle between the flux rope axis and the ecliptic plane, ϕ is the angle from the antisunward direction anticlockwise to the projection of the axis direction onto the ecliptic plane, and B_0 is the field strength along the flux rope axis.

The ~80° difference in latitude and ~65° difference in longitude of the flux rope axis between MESSENGER and STEREO A imply a significant rotation of the flux rope during propagation. We discuss in detail the likely causes of this rotation in section 4. Although we use one of the simplest models for the magnetic field reconstruction, we consider the result that the flux rope orientation changed between MESSENGER and STEREO A to be very robust. This is because the dominant component of the magnetic field and the sense of rotation of the B_T and B_N components differ at MESSENGER and STEREO A, as shown in Figures 2 and 3.

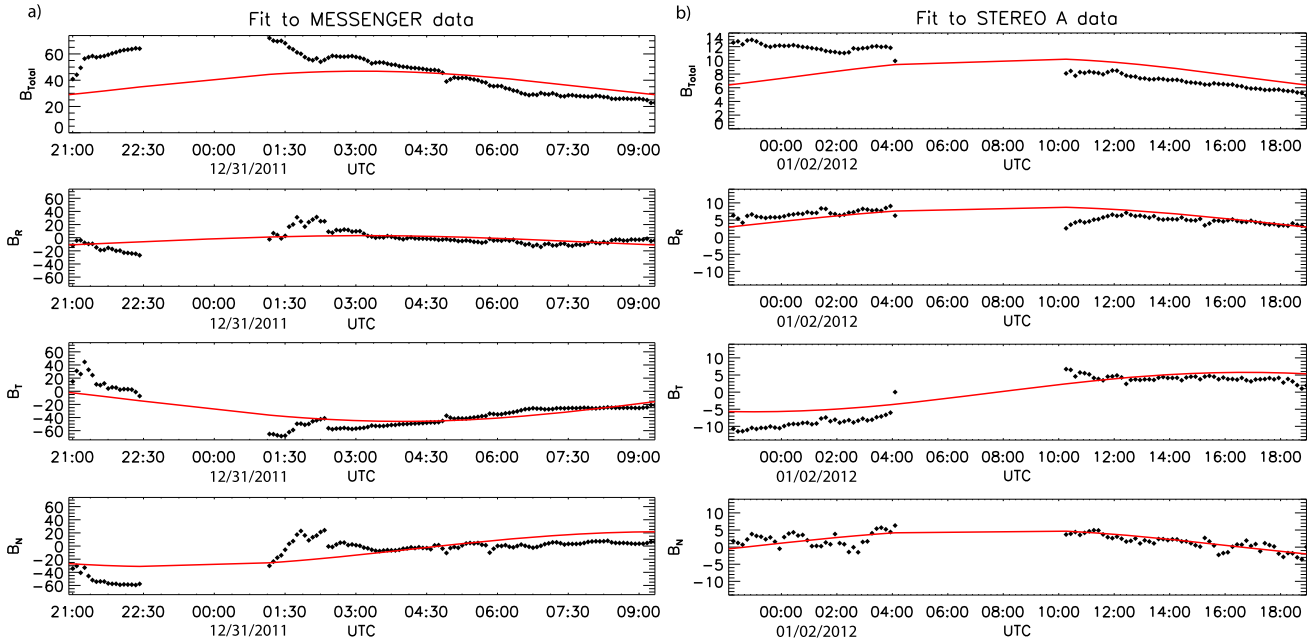

Figure 5. Force-free field constant α fits to binned (a) MESSENGER and (b) STEREO A magnetic field data. The fit results yielded left-handed flux ropes at both spacecraft, with flux rope parameters at MESSENGER of $\theta = -12.3^\circ \pm 0.4^\circ$, $\phi = 131^\circ \pm 1^\circ$, and $B_0 = 55.9 \pm 0.5$ nT and at STEREO A of $\theta = 66^\circ \pm 5^\circ$, $\phi = 197^\circ \pm 8^\circ$, and $B_0 = 12.3 \pm 0.5$ nT.

The force-free fitting also yielded $B_0 \propto r^{-1.83}$ where r is heliocentric distance, in good agreement with results obtained from the statistical study on all the ICMEs observed at MESSENGER by *Winslow et al.* [2015] and with other past studies using Helios data [e.g., *Gulisano et al.*, 2010]. The factor of ~5 decrease in the flux rope axial field strength is a clear indication of expansion of the cloud as it propagates from Mercury to 1 AU. An impact parameter of ~0.5 was obtained at both spacecraft, where the impact parameter is defined as the distance of closest approach of the spacecraft to the flux rope axis normalized by the radius of the flux rope. It is also worth mentioning that the fits had low χ^2 values of 0.09 at MESSENGER and 0.06 at STEREO A, indicating good quality fits at both spacecraft.

From the time of the CME launch at the Sun, the Sun-Mercury distance, and the arrival time at Mercury we can determine the average ICME speed between the Sun and Mercury. We can similarly obtain an average ICME speed between Mercury and STEREO A. Our results indicate an average shock speed from the Sun to Mercury of ~710 km s^{-1}, while from Mercury to STEREO A we find an average shock transit speed of ~500 km s^{-1}. At STEREO A this yields a ~50 km s^{-1} overestimate of the ICME shock speed, as Figure 3 shows the in situ measured speed to be ~450 km s^{-1}.

We can also estimate the ICME speed from the drag-based model [*Vršnak et al.*, 2013] available online at http://oh.geof.unizg.hr/DBM/dbm.php. The drag-based model assumes that after initial CME acceleration, aerodynamic drag is the dominant force acting on the CME. We used the following parameter values for the drag-based model: CME takeoff date and time 29 December 2011 21:11:00 at 20 R_{Sun}, initial CME speed of 750 km s^{-1}, solar wind speed of 350 km s^{-1}, and γ, the drag parameter, of 0.1×10^{-7}. At Mercury, at 0.42 AU, the model yields an ICME arrival time at 30 December 2011 16:29:00 with a speed of 663 km s^{-1}, which matches the MESSENGER observed arrival time perfectly. Interestingly, if we assume the same drag parameter value throughout propagation all the way to 1 AU, we find an arrival time of 1 January 2012 08:03:00 with a speed of 566 km s^{-1} at 1 AU. This yields a 5 h earlier arrival time than what was actually observed, and the speed is about 100 km s^{-1} faster than what is observed by STEREO A. This suggests that likely due to the ICME interacting with corotating structures in the Mercury-to-STEREO A transit space, it may not be appropriate to use the same drag parameter for the entire propagation distance. If we use a drag parameter value of 0.18×10^{-7} for estimating the ICME arrival to 1 AU, we find an arrival time of 13:31:00 with a speed of 500 km s^{-1} at STEREO A. This is only ~10 min off the arrival time and 50 km s^{-1} off the measured speed. Additionally, this scenario implies an ICME speed of 612 km s^{-1} at MESSENGER, which together with the previous scenario yields an

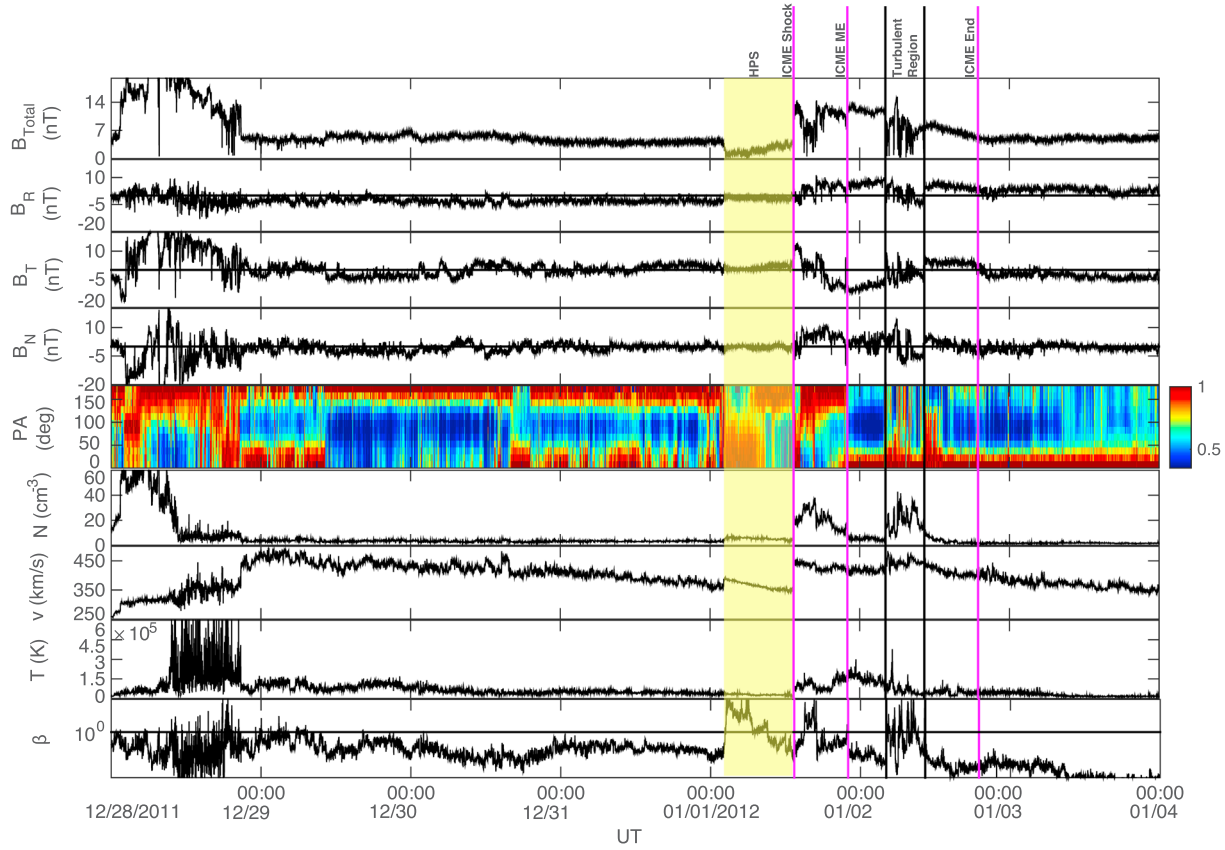

Figure 6. STEREO A magnetic field and plasma data a few days before and after the ICME. The panels are the same as in Figure 4, and the labeling of the vertical lines are the same as in Figure 3. The highlighted yellow region marks the beginning portion of the heliospheric plasma sheet (HPS).

upper and lower bound for the ICME speed at MESSENGER of 640 ± 25 km s^{-1}. Taking the ICME speed at Mercury to be 640 km s^{-1} from the drag-based model and the ICME speed to be 450 km/s as measured at 1 AU, we find a speed decrease of $\sim 30\%$, suggesting a significant speed decrease from Mercury to 1 AU, in line with our statistical study presented in *Winslow et al.* [2015].

4. Background Solar Wind Conditions

The significant change observed in the flux rope orientation implies strong interaction with the solar wind. In this section, we discuss both the measurements and simulations of the background solar wind in which the ICME propagated from MESSENGER to STEREO A. First, through simple inspection of the magnetic field measurements we can piece together a likely scenario. Magnetic field data at MESSENGER and STEREO A show that prior to the ICME shock arrival, the IMF B_R component was positive at Mercury and negative at STEREO A (see Figures 2 and 3). This is evidence for the ICME having encountered the heliospheric current sheet during propagation between Mercury and 1 AU. Furthermore, the magnetic field data alone yield insight as to when this might have happened. We can see that after the ICME passage, STEREO A reemerges into the interplanetary medium where the IMF B_R component is positive. Thus, just before the ICME arrived at STEREO A the spacecraft was in a negative polarity IMF, while just after the ICME passage the spacecraft was in a positive polarity IMF.

Further detail can be glimpsed from Figure 6, which shows STEREO A data a few days before and after (including) the ICME. Vertical lines demarcate the boundaries of the ICME (as described in section 2). Prior to the ICME shock arrival, there is a steep decrease in $|B|$, increase in density, increase in β, as well as a slow decrease in velocity starting at ~03:00 UT on 1 January 2012. During the same time, the suprathermal electrons exhibit a change first from somewhat bidirectional to mostly unidirectional flow opposite to the strahl and then back again to a strong strahl component. We also note that the iron charge state distribution shows a change from

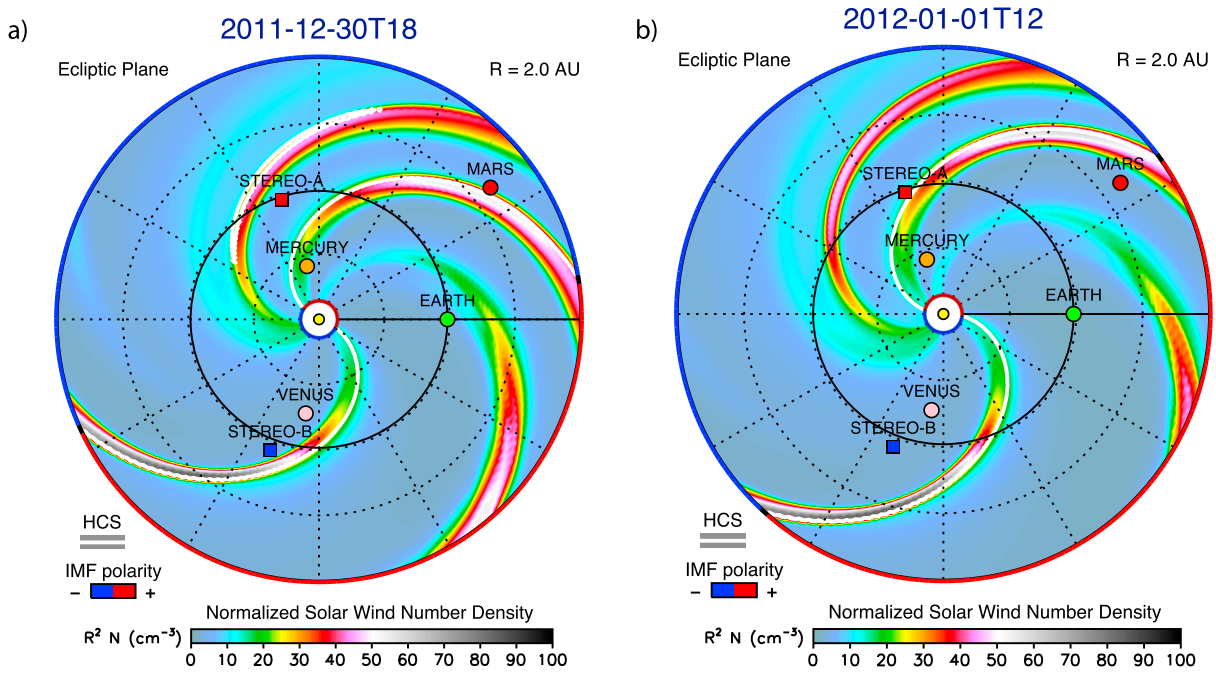

Figure 7. (a and b) ENLIL-MAS model simulated steady state solar wind conditions for two time steps: (a) at 18:00 UT on 30 December 2011, just after the ICME reached MESSENGER, and at (b) 12:00 UT on 1 January 2012, just before the ICME reached STEREO A. (a) The HPS/HCS had passed by Mercury prior to the ICME arrival, while (b) the HPS/HCS is about to reach STEREO A, very close to the time that the ICME also arrived.

an average value of 10 to an average value of 12 near 03:00 UT on 1 January (see Figure 3). An important property of ionic charge states is that they remain virtually constant after the freeze-in point (~10 R_S), and thus, they represent different sources for the plasma close to the Sun. We attribute all of these changes to the vicinity of an extended heliospheric plasma sheet (in which the HCS is embedded). All these changes come at the tail end of a high speed stream following a corotating interaction region (CIR) on 28 December 2011. The combination of signatures observed at the time before the ICME arrival, specifically the very low $|B|$ (<1 nT), increase in density and in β, suggest that the spacecraft encountered the HPS. This is further supported by the change in sign of B_R and the clear change in the suprathermal electron strahl direction from 180° to 0° during the ICME passage. These observations are directly in line with those by *Winterhalter et al.* [1994] of the HPS, which show that on average, the HCS is displaced from the center of the HPS in which it is embedded, as is the case here. Thus, the measurements suggest that the ICME encountered and overtook the HCS and part of the HPS before reaching STEREO A.

The linearly decreasing speed profile on 1 January has raised the possibility that this feature might be a small ICME as opposed to the HPS, with the measured low magnetic field magnitude being due to overexpansion. This is unlikely given the near-zero magnetic field value, the increase in plasma density, and the increased plasma β. We have also checked for possible CME candidates that could have resulted in an ICME prior to the 29 December ICME, with only two meeting the direction criteria. As these two CMEs (both launched on 27 December) are much smaller and fainter than the 29 December CME and, as they originate from 15° to 20° from disk center, they are unlikely to have resulted in strong and/or long-lasting disturbances in the solar wind at 1 AU as measured by STEREO A.

Steady state solar wind simulation results from the ENLIL model [*Odstrcil*, 2003] are shown in Figures 7a and 7b for two different times: just after the ICME reached Mercury and just before the ICME reached STEREO A. The simulations were run at the Community Coordinated Modeling Center for Carrington Rotation 2118, with the Magnetohydrodynamics outside A Sphere (MAS) coronal model [*Linker et al.*, 1999; *Mikic et al.*, 1999] and magnetogram data obtained from the Kitt Peak observatory. Both figures show normalized solar wind density in the ecliptic plane as a function of longitude. The IMF polarity is indicated as red (positive) or blue (negative) coloring of the circular border, and we note that the HCS is marked by the white line in the figures. The simulation results clearly show an HCS between Mercury and STEREO A, confirming the scenario gleaned from magnetic field data. They indicate the HCS having passed by Mercury prior to the ICME arrival, while at STEREO

A, the HCS arrives just after the ICME. The simulations also reveal that the HCS is embedded in the HPS, as seen by the region of high-density plasma following the HCS in Figures 7a and 7b. Based on these data and the simulations, we have a clearer picture of the sequence of events which transformed a relatively straightforward ICME and flux rope at MESSENGER into a highly disturbed one at STEREO A:

1. The ICME is ejected into positive polarity IMF and relatively undisturbed solar wind.
2. At Mercury, the passage of the HPS/HSC is observed in the magnetic field data at ~5:00 UT on 29 December 2011, ~1.5 days prior to the ICME arrival, so the ICME does not interact with it yet. Therefore, MESSENGER observes a fairly undisturbed ICME with a straightforward flux rope that has a latitudinal orientation close (within ~20°) to that expected from the GCS model of the CME soon after launch.
3. During propagation from Mercury to STEREO A, the ICME catches up to part of the HPS. It is likely that the turbulent region observed within the flux rope at STEREO A is highly compressed plasma from the HPS that was "engulfed" by the ICME. This complex structure at 1 AU (especially in light of the suprathermal electron data), compared with the measurements at MESSENGER, suggests that extensive magnetic reconnection took place between the ICME and the HPS/HCS magnetic fields. The ICME likely overtook the HCS just prior to reaching STEREO A. The complexity in the ICME composition at STEREO A that arose due to the ICME interacting with the HPS and HCS is further evidenced by the iron charge state data.

Similarly, in a recent paper, *Prise et al.* [2015] observe an ICME overtaking and merging with a CIR, although in their case this occurs further out in the solar system, between Mars' and Saturn's orbits. For our event, the observations and simulations paint the picture of an ICME with a fairly simple initial structure that was made significantly more complex due to interaction with existing disturbances in the solar wind. Our example provides direct evidence for solar wind induced alteration of the magnetic topology within ICMEs.

5. Discussion and Conclusions

In this paper we present a case study of the evolution of a CME ejected from the Sun on 29 December 2011 as it propagates from the Sun to Mercury and then to 1 AU. At MESSENGER, magnetic field measurements present a fairly simple ICME structure with ordered magnetic fields indicative of a MC. Despite the near-perfect longitudinal alignment between MESSENGER and STEREO A during the time the CME propagates from Mercury to 1 AU, STEREO A data indicate a significantly altered and more disturbed ICME.

The three most striking features of this ICME are (1) the significantly changed magnetic topology between MESSENGER and STEREO A (seen both in the magnetic field measurements and from the flux rope fitting); (2) the enclosed turbulent region within the center of the ICME observed at STEREO A but not at MESSENGER; and (3) the clear variation at STEREO A from counter-streaming to unidirectional suprathermal electron flows in the turbulent region, implying variation between closed and open magnetic field lines as the spacecraft travels through this reconnection region. These features illustrate the increased complexity in ICME structure during propagation from 0.42 AU at MESSENGER to 0.96 AU at STEREO A due to strong interaction of the ICME with the solar wind.

Significant alteration of the magnetic topology requires reconnection to occur either within the ICME or between the ICME and the IMF. *Gosling et al.* [1995] first discussed how sustained three-dimensional reconnection close to the Sun between different sheared or skewed coronal loops can alter the flux rope topology and produce field lines within CMEs that are open and/or are connected to the outer heliosphere at both ends. Their Figure 4 exemplifies several different magnetic topologies that can arise in CMEs that have undergone three-dimensional reconnection. In addition, based on observational evidence and theoretical considerations, *Fermo et al.* [2014] showed that any deviation from the lowest energy state of a flux rope, the so-called Taylor state, will result in reconnection occurring within the interior of the flux rope.

The ICME event presented in this paper likely has undergone three-dimensional reconnection, specifically interchange reconnection [e.g., *Lugaz et al.*, 2011; *Masson et al.*, 2013], and thus, the reconnection did not occur within the ICME itself but with the magnetic fields of the HPS/HCS in the solar wind. The short duration, multiple successions of bidirectional and unidirectional suprathermal electron flows in the turbulent region are indicative of the spacecraft traversing a succession of closed and open field lines within this short time frame. We infer that most likely the closed field lines of the ICME, interchange reconnected with the open field lines of the HPS in transit between ~0.4 and ~1 AU, thereby opening up some of the closed ICME field lines. Figure 8 shows a simplified cartoon example of the possible reconnection scenario between the flux

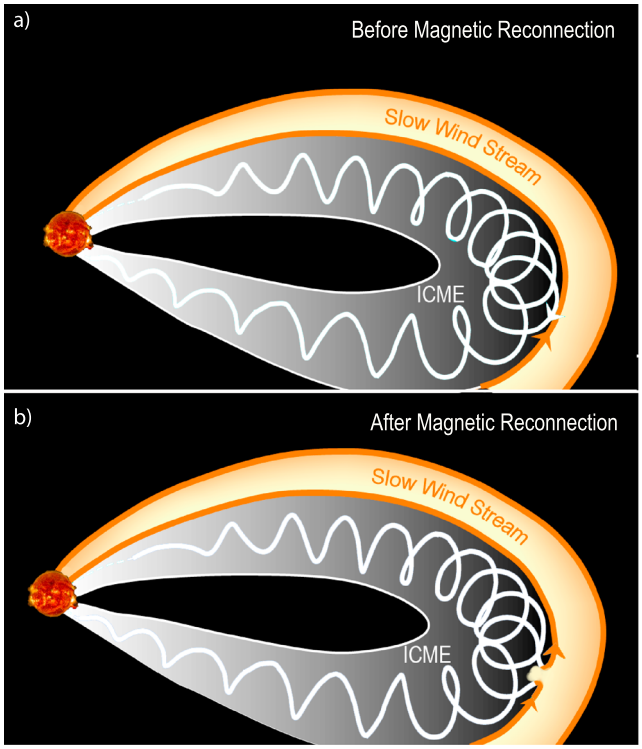

Figure 8. (a–b) Cartoon depiction of possible reconnection between the ICME flux rope and HPS field lines. After reconnection, the ICME magnetic topology is altered and some HPS plasma is now on ICME field lines.

rope and the HPS field line. It has been shown both through observations [e.g., *Dasso et al.*, 2006, 2007; *Möstl et al.*, 2008; *Ruffenach et al.*, 2012] and MHD simulations [e.g., *Schmidt and Cargill*, 2003; *Taubenschuss et al.*, 2010] that reconnection between the front of a magnetic cloud and the IMF alters the flux rope topology and causes erosion of the ICME. Through a large statistical study, *Ruffenach et al.* [2015] showed that MCs can be eroded at both the front and rear ends in similar proportions, i.e., reconnection between the flux rope and the IMF can occur at the front or the rear of the ICME.

The event discussed in this paper, however, seems to differ from these scenarios in that the reconnected region between the HPS and ICME lies at the center of the ME as opposed to the front or the rear. A possible explanation is that due to reconnection between the front of the ICME and the HPS magnetic field, not only did the overall magnetic topology of the flux rope change, but part of the wind stream within the HPS became enveloped by the expanding ME. The turbulent region observed within the flux rope at STEREO A appears to be an inclusion of HPS plasma. A possible way that this could have occurred is that the ICME "engulfed" the HPS by expanding around it in latitude. Due to the higher density of the HPS in the ecliptic, the front central part of the ICME likely interacted with the HPS, which is where the reconnection occurred, but the flanks of the ICME may have been deflected around the HPS in latitude and later expanded back to the ecliptic. This scenario could explain the relative central appearance of the reconnected region within the flux rope and the large change in overall flux rope orientation. We note that it is possible that to some extent the relative central appearance of the turbulent region within the ME is caused by a limitation in the observations due to the large-scale three-dimensional nature of the ICME compared to the one-dimensional nature of the spacecraft crossing. However, some amount of envelopment of HPS plasma by the ME is required by the measurements regardless of the crossing geometry. Further modeling work is necessary to test whether the expansion of the ME, especially in latitude, can account for the relative central appearance of the reconnection region within the flux rope.

The idea that complexity in ICME structure increases with heliocentric distance due to prolonged interaction with the solar wind has been studied in the past. For example, the fact that the MC fraction at 1 AU displays a strong solar cycle dependence [*Richardson and Cane*, 2010], with the highest MC fraction observed at solar minimum when the Sun is most quiet, is an indication that the MC fraction does reflect to some extent

interaction between ICMEs and other solar transients in the solar wind during transit [*Richardson and Cane*, 2004]. Thus, the relative decrease in MC fraction with heliocentric distance can be used as a proxy measure of increasing complexity in ICMEs.

Analyzing a small subset of inner heliospheric observations by the Helios spacecraft between 1979 and 1981, *Bothmer and Schwenn* [1996] found that 7 out of 17 (41%) ICMEs exhibited MC characteristics. Indirect evidence suggests that a large fraction of the 61 ICMEs cataloged by *Winslow et al.* [2015] between 2011 and 2014 at Mercury's orbit are MCs, although an exact number cannot be determined due to the lack of solar wind plasma observations with MESSENGER. At 1 AU, over the solar cycle, approximately one third of ICMEs show MC signatures [*Gosling*, 1990; *Richardson and Cane*, 2010]. Beyond Earth's orbit, *Rodriguez et al.* [2004] using Ulysses observations between 1 and 5 AU found 40 out of 148 (27%) ICMEs to be MCs. Overall, this is a modest drop in MC fraction from ~0.3 to 5 AU and a slight indication of increased complexity, incorporating studies of varying statistical significance and during different solar cycles. Studying the evolution of complexity in ICMEs with heliocentric distance requires multipoint in situ magnetic field and or plasma data, making such studies difficult to attain in the past due to lack of adequate measurements. The recently completed MESSENGER mission and the upcoming Solar Probe Plus and Solar Orbiter missions to the innermost heliosphere in the next few years should help in this regard. Our paper provides a concrete example of increased complexity in ICME structure from Mercury to 1 AU solely due to interaction of the ICME with an HCS and HPS in the solar wind.

This increase in complexity and large change in magnetic topology during propagation has significant implications not only for ICME evolution in the solar wind but also for geomagnetic storm forecasting. The magnetic field direction and duration in the ICME largely determines the likelihood of geomagnetic storm onset. Our results show that depending on the timing of ICME eruptions and the presence of corotating structures in the solar wind, magnetic field measurements in the innermost heliosphere may not be accurate in predicting ICME magnetic field direction at the Earth. However, the timing and location of HPS' and HCS' can be modeled fairly accurately due their corotating nature [*Jian et al.*, 2015]. Thus, geomagnetic storm forecasting based on in situ magnetic field data upstream of the Earth may still be accurate at times when corotating structures are not present in the ICME transit path from the Sun to 1 AU. These results also highlight the need for a statistical study to evaluate the frequency of significant alterations in flux rope orientation during propagation between the innermost heliosphere and 1 AU.

Acknowledgments

Support for this work was provided by the NASA Lunar Reconnaissance Orbiter Project (NASA contract NNG11PA03C), as well as various NASA grants (EMMREM, grant NNX07AC14G; C-SWEPA, grant NNX07AC14G; DoSEN, grant NNX13AC89G; DREAM, grant NNX10AB17A; and DREAM2; grant NNX14AG13A) and two NSF grants (Sun-2-Ice, grant AGS1135432 and grant AGS1622352). We also thank the International Space Science Institute for supporting the Research Team: Radiation Interactions at Planetary Bodies (http://www.issibern.ch/teams/interactplanetbody/). R. W. acknowledges support from NASA grant NNX15AW31G and NSF grant AGS1622352. N.L. acknowledges support from NASA grants NNX15AB87G and NNX13AP52G. We also acknowledge support from the STEREO-FARSIDE grant (NNX13AP52G) to the University of New Hampshire. MESSENGER data are available on the Planetary Data System (https://pds.jpl.nasa.gov). STEREO data are available on the Space Physics Data Facility (http://cdaweb.gsfc.nasa.gov). Simulation results (run number Reka_Winslow_110515_SH_1) have been provided by special request from the Community Coordinated Modeling Center at Goddard Space Flight Center through their public Runs on Request system (http://ccmc.gsfc.nasa.gov). The MAS model was developed by J. Linker, Z. Mikic, R. Lionello, and P. Riley and the ENLIL Model was developed by D. Odstrcil. We thank two anonymous reviewers for their comments on the paper.

References

Andrews, G. B., et al. (2007), The energetic particle and plasma spectrometer instrument on the MESSENGER spacecraft, *Space Sci. Rev.*, *131*, 523–556.

Bothmer, V., and R. Schwenn (1996), Signatures of fast CMEs in interplanetary space, *Adv. Space Res.*, *17*, 319–322.

Burlaga, L. F. (1988), Magnetic clouds and force-free fields with constant alpha, *J. Geophys. Res.*, *93*, 7217, doi:10.1029/JA093iA07p07217.

Cane, H. V., and I. G. Richardson (2003), Interplanetary coronal mass ejections in the near-Earth solar wind during 1996–2002, *J. Geophys. Res.*, *108*, 1156, doi:10.1029/2002JA009817.

Dasso, S., C. H. Mandrini, P. Démoulin, and M. L. Luoni (2006), A new model-independent method to compute magnetic helicity in magnetic clouds, *Astron. Astrophys.*, *455*, 349–359, doi:10.1051/0004-6361:20064806.

Dasso, S., M. S. Nakwacki, P. Demoulin, and C. H. Mandrini (2007), Progressive transformation of a flux rope to an ICME, *Sol. Phys.*, *244*, 115–137, doi:10.1007/s11207-007-9034-2.

Farrugia, C. J., I. G. Richardson, L. F. Burlaga, R. P. Lepping, and V. A. Osherovich (1993), Simultaneous observations of solar MeV particles in a magnetic cloud and in the Earth's northern tail lobe: Implications for the global field line topology of magnetic clouds and for the entry of solar particles into the magnetosphere during cloud passage, *J. Geophys. Res.*, *98*, 15,497–15,507.

Farrugia, C. J., L. F. Burlaga, and R. P. Lepping (1997), Magnetic clouds and the quiet/storm effect at Earth: A review, in *Magnetic Storms, Geophys. Monogr. Ser.*, vol. 98, edited by B. T. Tsurutani et al., p. 91, AGU, Washington, D. C.

Fermo, R. L., M. Opher, and J. F. Drake (2014), Magnetic reconnection in the interior of interplanetary coronal mass ejections, *Phys. Rev. Lett.*, *113*, 31101, doi:10.1103/PhysRevLett.113.031101.

Fox, N. J., et al. (2015), The Solar Probe Plus mission: Humanity's first visit to our star, *Space Sci. Rev.*, 1–42, doi:10.1007/s11214-015-0211-6.

Galvin, A. B., et al. (2008), The Plasma and Suprathermal Ion Composition (PLASTIC) investigation on the STEREO observatories, *Space Sci. Rev.*, *136*, 437–486, doi:10.1007/s11214-007-9296-x.

Gershman, D. J., et al. (2012), Solar wind alpha particles and heavy ions in the inner heliosphere observed with MESSENGER, *J. Geophys. Res.*, *117*, A00M02, doi:10.1029/2012JA017829.

Good, S. W., R. J. Forsyth, J. M. Raines, D. J. Gershman, J. A. Slavin, and T. H. Zurbuchen (2015), Radial evolution of a magnetic cloud: MESSENGER, STEREO, and Venus Express observations, *Astrophys. J.*, *807*, 177, doi:10.1088/0004-637X/807/2/177.

Gonzalez, W. D., and B. T. Tsurutani (1987), Criteria of interplanetary parameters causing intense magnetic storms ($Dst < -100nT$), *Planet. Space Sci.*, *35*, 1101–1109.

Gosling, J. T. (1990), Coronal mass ejections and magnetic flux ropes in interplanetary space, in *Physics of Magnetic Flux Ropes, Geophys. Monogr.*, vol. 58, edited by E. R. Priest and L. C. Lee, pp. 343–364, AGU, Washington, D. C.

Gosling, J. T., J. Birn, and M. Hesse (1995), Three-dimensional magnetic reconnection and the magnetic topology of coronal mass ejection events, *Geophys. Res. Lett.*, *22*, 869–872.

Gosling, J. T., and V. J. Pizzo (1999), Formation and evolution of corotating interaction regions and their three dimensional structure, *Space Sci. Rev.*, *89*, 21–52.

Gulisano, A. M., P. Démoulin, S. Dasso, M. E. Ruiz, and E. Marsch (2010), Global and local expansion of magnetic clouds in the inner heliosphere, *Astron. Astrophys.*, *509*, A39.
Jian, L. K., P. J. MacNeice, A. Taktakishvili, D. Odstrcil, B. Jackson, H.-S. Yu, P. Riley, I. V. Sokolov, and R. M. Evans (2015), Validation for solar wind prediction at Earth: Comparison of coronal and heliospheric models installed at the CCMC, *Space Weather*, *13*, 316–338, doi:10.1002/2015SW001174.
Kay, C., M. Opher, and R. M. Evans (2013), Forecasting a coronal mass ejection's altered trajectory: ForeCAT, *Astrophys. J.*, *775*, 5.
Kay, C., M. Opher, and R. M. Evans (2015), Global trends of CME deflections based on CME and solar parameters, *Astrophys. J.*, *805*, 168.
Kliem, B., T. Török, and W. T. Thompson (2012), A parametric study of erupting flux rope rotation. Modeling the "Cartwheel CME" on 9 April 2008, *Sol. Phys.*, *281*, 137–166.
Kubicka, M., C. Möstl, T. Rollett, L. Feng, J. P. Eastwood, and P. D. Boakes (2015), Prediction of geomagnetic storm strength from inner heliospheric in situ observations, presented at 2015 Fall Meeting, SH21B-2408, AGU, San Francisco, Calif., 14–18 Dec.
Lavraud, B., et al. (2014), Geo-effectiveness and radial dependence of magnetic cloud erosion by magnetic reconnection, *J. Geophys. Res. Space Physics*, *119*, 26–35, doi:10.1002/2013JA019154.
Lepping, R. P., L. F. Burlaga, and J. A. Jones (1990), Magnetic field structure of interplanetary magnetic clouds at 1 AU, *J. Geophys. Res.*, *95*, 11,957–11,965.
Lindsay, G. M., C. T. Russell, and J. G. Luhmann (1995), Coronal mass ejection and stream interaction region characteristics and their potential geomagnetic effectiveness, *J. Geophys. Res.*, *100*, 16,999–17,013.
Linker, J., et al. (1999), Magnetohydrodynamic modeling of the solar corona during Whole Sun Month, *J. Geophys. Res.*, *104*, 9809–9830.
Luhmann, J. G., et al. (2008), STEREO IMPACT investigation goals, measurements, and data products overview, *Space Sci. Rev.*, *136*, 117–184, doi:10.1007/s11214-007-9170-x.
Lugaz, N., C. Downs, K. Shibata, I. I. Roussev, A. Asai, and T. I. Gombosi (2011), Numerical investigation of a coronal mass ejection from an anemone active region: Reconnection and deflection of the 2005 August 22 eruption, *Astrophys. J.*, *738*, 127, doi:10.1088/0004-637X/738/2/127.
Lynch, B. J., T. H. Zurbuchen, L. A. Fisk, and S. K. Antiochos (2003), Internal structure of magnetic clouds: Plasma and composition, *J. Geophys. Res.*, *108*, 1239, doi:10.1029/2002JA009591.
Lynch, B. J., S. K. Antiochos, Y. Li, J. G. Luhmann, and C. R. DeVore (2009), Rotation of coronal mass ejections during eruption, *Astrophys. J.*, *697*, 1918.
Manchester, W. B., IV, et al. (2004), Modeling a space weather event from the Sun to the Earth: CME generation and interplanetary propagation, *J. Geophys. Res.*, *109*, A02107.
Manchester, W. B., IV, et al. (2005), Coronal mass ejection shock and sheath structures relevant to particle acceleration, *Astrophys. J.*, *622*, 1225–1239.
Masson, S., S. K. Antiochos, and C. R. DeVore (2013), A model for the escape of solar-flare-accelerated particles, *Astrophys. J.*, *771*, 82, doi:10.1088/0004-637X/771/2/82.
Mikic, Z., J. A. Linker, D. D. Schnack, R. Lionell o, and A. Tarditi (1999), Magnetohydrodynamic modeling of the global solar corona, *Phys. Plasmas*, *6*, 2217–2224.
Möstl, C., C. Miklenic, C. J. Farrugia, M. Temmer, A. Veronig, A. B. Galvin, and H. K. Biernat (2008), Two-spacecraft reconstruction of a magnetic cloud and comparison to its solar source, *Ann. Geophys.*, *26*, 3139–3152, doi:10.5194/angeo-26-3139-2008.
Möstl, C., et al. (2012), Multi-point shock and flux rope analysis of multiple interplanetary coronal mass ejections around 2010 August 1 in the inner heliosphere, *Astrophys. J.*, *758*, 10.
Müller, D., and O. C. St. Cyr (2013), The solar orbiter mission, *Proc. SPIE*, *8862*, 88620E.
Nieves-Chinchilla, T., R. Colaninno, A. Vourlidas, A. Szabo, R. P. Lepping, S. A. Boardsen, B. J. Anderson, and H. Korth (2012), Remote and in situ observations of an unusual Earth-directed coronal mass ejection from multiple viewpoints, *J. Geophys. Res.*, *117*, A06106, doi:10.1029/2011JA017243.
Odstrcil, D. (2003), Modeling 3-D solar wind structure, *Adv. Space Res.*, *32*, 497–506.
Palmerio, E., E. K. J. Kilpua, and N. P. Savani (2016), Planar magnetic structures in coronal mass ejection-driven sheath regions, *Ann. Geophys.*, *34*, 313–322.
Prise, A. J., L. K. Harra, S. A. Matthews, C. S. Arridge, and N. Achilleos (2015), Analysis of a coronal mass ejection and corotating interaction region as they travel from the Sun passing Venus, Earth, Mars, and Saturn, *J. Geophys. Res. Space Physics*, *120*, 1566–1588, doi:10.1002/2014JA020256.
Richardson, I. G., and H. V. Cane (2004), The fraction of interplanetary coronal mass ejections that are magnetic clouds: Evidence for a solar cycle variation, *Geophys. Res. Lett.*, *31*, L18804, doi:10.1029/2004GL020958.
Richardson, I. G., and H. V. Cane (2010), Near-Earth interplanetary coronal mass ejections during solar cycle 23 (1996–2009): Catalog and summary of properties, *Sol. Phys.*, *264*, 189–237.
Rodriguez, L., J. Woch, N. Krupp, M. Fränz, R. von Steiger, R. J. Forsyth, D. B. Reisenfeld, and K.-H. Glassmeier (2004), A statistical study of oxygen freezing-in temperature and energetic particles inside magnetic clouds observed by Ulysses, *J. Geophys. Res.*, *109*, A01108, doi:10.1029/2003JA010156.
Ruffenach, A., et al. (2012), Multispacecraft observation of magnetic cloud erosion by magnetic reconnection during propagation, *J. Geophys. Res.*, *117*, A09101, doi:10.1029/2012JA017624.
Ruffenach, A., et al. (2015), Statistical study of magnetic cloud erosion by magnetic reconnection, *J. Geophys. Res. Space Physics*, *120*, 43–60, doi:10.1002/2014JA020628.
Rouillard, A. P., et al. (2009), A solar storm observed from the Sun to Venus using the STEREO, Venus Express, and MESSENGER spacecraft, *J. Geophys. Res.*, *114*, A07106, doi:10.1029/2008JA014034.
Russell, C. T., R. L. McPherron, and R. K. Burton (1974), On the cause of geomagnetic storms, *J. Geophys. Res.*, *79*, 1105–1109.
Schmidt, J. M., and P. J. Cargill (2003), Magnetic reconnection between a magnetic cloud and the solar wind magnetic field, *J. Geophys. Res.*, *108*, 1023, doi:10.1029/2002JA009325.
Schwartz, S. J. (1998), Shock and discontinuity normals, mach numbers, and related parameters, in *Analysis Methods for Multi-Spacecraft Data*, vol. 1, edited by G. Paschmann and P. Daly, pp. 249–270, ISSI Sci. Rep. Ser., ESA/ISSI.
Singh, A. K., D. Siingh, and R. P. Singh (2010), Space weather: Physics, effects, and predictability, *Surv. Geophys.*, *31*, 581–638, doi:10.1007/s10712-010-9103-1.
Taubenschuss, U., N. V. Erkaev, H. K. Biernat, C. J. Farrugia, C. Möst, and U. V. Amerstorfer (2010), The role of magnetic handedness in magnetic cloud propagation, *Ann. Geophys.*, *28*, 1075–1100, doi:10.5194/ angeo-28-1075-2010.
Thernisien, A. F. R. (2011), Implementation of graduated cylindrical shell model for the three-dimensional reconstruction of coronal mass ejections, *Astrophys. J. Suppl. Ser.*, *194*, 33.

Thernisien, A. F. R., R. A. Howard, and A. Vourlidas (2006), Modeling of flux rope coronal mass ejections, *Astrophys. J.*, *652*, 763–773.
Tsurutani, B. T., B. E. Goldstein, W. D. Gonzalez, and F. Tang (1988), Comment on — A new method of forecasting geomagnetic activity and proton showers, by A. Hewish and P. J. Duffet-Smith, *Planet. Space Sci.*, *36*, 205–206.
Vršnak, B., et al. (2013), Propagation of interplanetary coronal mass ejections: The drag-based model, *Sol. Phys.*, *285*, 295–315.
Wang, Y., B. Wang, C. Shen, F. Shen, and N. Lugaz (2014), Deflected propagation of a coronal mass ejection from the corona to interplanetary space, *J. Geophys. Res. Space Physics*, *119*, 5117–5132, doi:10.1002/2013JA019537.
Winslow, R. M., N. Lugaz, L. C. Philpott, N. A. Schwadron, C. J. Farrugia, B. J. Anderson, and C. W. Smith (2015), Interplanetary coronal mass ejections from MESSENGER orbital observations at Mercury, *J. Geophys. Res. Space Physics*, *120*, 6101–6118, doi:10.1002/2015JA021200.
Winterhalter, D., E. J. Smith, M. E. Burton, N. Murphy, and D. J. McComas (1994), The heliospheric plasma sheet, *J. Geophys. Res.*, *99*, 6667–6680.
Zhang, J.-Ch., M. W. Liemohn, J. U. Kozyra, B. J. Lynch, and T. H. Zurbuchen (2004), A statistical study of the geoeffectiveness of magnetic clouds during high solar activity years, *J. Geophys. Res.*, *109*, A09101, doi:10.1029/2004JA010410.
Zurbuchen, T. H., and I. G. Richardson (2006), In-situ solar wind and magnetic field signatures of interplanetary coronal mass ejections, *Space Sci. Rev.*, *123*, 31–43.